Numerical comparison between single PCM and multi-stage PCM based high temperature thermal energy storage for CSP tower plants

Article *in* Applied Thermal Engineering · May 2018

DOI: 10.1016/j.applthermaleng.2018.04.122

CITATIONS
6

READS
183

3 authors, including:

K. E. Elfeky
Xi'an Jiaotong University
15 PUBLICATIONS **69** CITATIONS

SEE PROFILE

Naveed Ahmed
Xi'an Jiaotong University
7 PUBLICATIONS **24** CITATIONS

SEE PROFILE

Applied Thermal Engineering 139 (2018) 609–622

Contents lists available at ScienceDirect

Applied Thermal Engineering

journal homepage: www.elsevier.com/locate/apthermeng

Research Paper

Numerical comparison between single PCM and multi-stage PCM based high temperature thermal energy storage for CSP tower plants

K.E. Elfeky, N. Ahmed, Qiuwang Wang*

Key Laboratory of Thermo-Fluid Science and Engineering, Ministry of Education, School of Energy and Power Engineering, Xi'an Jiaotong University, Xi'an, Shaanxi 710049, PR China

HIGHLIGHTS

- Thermal behaviors of single and multi PCM thermocline storage are presented.
- Temperature response and phase change process within capsules are revealed.
- Energy analysis of thermocline latent heat thermal storage systems is presented.
- Multi-stage PCM is a promising solution to store thermal energy for CSP plants.

ARTICLE INFO

Keywords:
Spherical capsule
Phase change material
Melting temperature
Concentrating solar power

ABSTRACT

This paper is aimed at analyzing the behavior of a packed bed latent heat thermal energy storage system in concentrating solar power (CSP). One way of improving the performance of a latent thermal energy storage system is by implementing the multiple phase change materials (PCMs) design. The behavior of a packed bed latent heat thermal energy storage system at different cases is numerically analyzed. The molten salt is considered for the heat transfer fluid (HTF) with phase change material (PCM) capsules as the filler. In this design, spherical capsules filled with PCMs of different thermo-physical properties are used. The capsules are packed in the bed at different sections based on the PCM melting temperature. The model developed using the Concentric-Dispersion (C-D) equations. The governing equations are solved in MATLAB, and the results obtained are validated against experimental data from the literature. The performance of the systems is calculated. The results show that the three-stage PCMs system with different melting point exhibited the highest energy and exergy efficiency during a charging discharging cycle. Moreover, results show that the three-stage PCMs unit can improve the heat transfer rate greatly and shorten the heat storage time effectively.

1. Introduction

Concentrating solar power (CSP) plants rely on thermal energy from the sun to generate electricity. The integration of a thermal energy storage unit eliminates the need for any fossil fuel backup to compensate for cloud transients and diurnal insolation variations. Without any fossil fuel backup, CSP plants can be considered to be the clean energy source of the future and have the potential to replace greenhouse gas emitting fossil-fueled power plants. Several methods of storing thermal energy for different temperature ranges have been discussed and reviewed [1,2].

A Presently, to store thermal energy using latent heat storage in a packed bed is the most attractive method. In a packed bed thermal storage system, a large amount of heat transfer surface area can be contained in a small volume, and the irregular flow that exists in the voids of the bed enhances transport through turbulent mixing [3]. However, latent thermal energy system suffers from low thermal conductivity of the PCMs. This leads to low charging and discharging rates. Different methods have been proposed to overcome such drawback. Encapsulation of the PCM within the heat transfer fluid is one of the method used to enhance the heat transfer process; thus helping to improve the dynamic performance of a latent heat thermal energy storage system [4]. During the charging process, the heat transfer rate is a function of temperature difference between the HTF and the PCM; less heat transfer rate is expected at the downstream sections of the bed. High heat transfer rate can be maintained if the series of PCMs with a decreasing melting temperature along the bed are used. During the discharging process, the HTF needs to flow in the opposite direction to

* Corresponding author.
E-mail address: wangqw@mail.xjtu.edu.cn (Q. Wang).

https://doi.org/10.1016/j.applthermaleng.2018.04.122
Received 8 February 2018; Received in revised form 24 April 2018; Accepted 26 April 2018
Available online 04 May 2018
1359-4311/

Nomenclature

Latin characters

A_{bed}	area of bed cross section, m^2
c_p	specific heat capacity, $J{\cdot}kg^{-1}{\cdot}K^{-1}$
D_{bed}	diameter of storage tank, m
d_p	diameter of PCM spheres, m
d_r	reference diameter, m
d_j	diameter of insulation layer j, m
E_{stored}	energy stored in the PCM particles, J
E_{pump}	pumping energy, J
E_{input}	input energy, J
$E_{outflow}$	the energy extracted from the tank, J
$Ex_{rec,f,net}$	net exergy recovered, J
$Ex_{sup,f,net}$	net exergy supplied, J
E^{max}_{stored}	maximum theoretical energy can be stored, J
g	gravity, $m{\cdot}s^{-1}$
H	storage tank height, m
h	heat transfer coefficient, $W{\cdot}m^{-2}{\cdot}K^{-1}$
h_f	volumetric heat transfer coefficient between fluid and solid, $W{\cdot}m^{-2}{\cdot}K^{-1}$
h_w	volumetric heat transfer coefficient between tank and ambience, $W{\cdot}m^{-2}{\cdot}K^{-1}$
k	thermal conductivity, $W{\cdot}m^{-1}{\cdot}K^{-1}$
Lhm	latent heat of melting, $J{\cdot}kg^{-1}$
$\dot{m}$	mass flow rate, $kg{\cdot}s^{-1}$
m	mass, kg
Nu	Nusselt number
N_x	nodes in the axial direction
n	number of insulations
Pr	Prandtl number
ΔP	pressure drop, Pa
Ra	Rayleigh number
Re	Reynolds number
R_x	nodes within each sphere
r	radius of PCM spheres, m
T	temperature, K
T_{p2}	peak temperature of the PCM during the solid–liquid transition, K
T_{p1}	peak temperature of the PCM during the solid–solid transition, K
T_{ini}	initial bed temperature, K
T_{inf}	ambient temperature, K
ΔT	temperature difference, K
t	time, s
u_f	fluid velocity, $m{\cdot}s^{-1}$
x	axial direction

Greek symbols

ε	average bed porosity
μ	dynamic viscosity, $kg{\cdot}m^{-1}{\cdot}s^{-1}$
ν	kinematic viscosity, $m^2{\cdot}s^{-1}$
α	axial thermal diffusivity, $m^2{\cdot}s^{-1}$
η	energy efficiency
η_{II}	overall exergy efficiency
γ	utilization ratio
ρ	density, $kg{\cdot}m^{-3}$
σ	capacity ratio
β	volumetric heat expansion coefficient of fluid, K^{-1}

Subscripts

ave	average
ch	charging
disch	discharging
f	fluid
in	inlet
j	index for insulations
l	liquid PCM
out	outlet
p	particles
rec	recovered
sup	supplied
s	solid

Superscripts

i	index for time step
max	maximum

Abbreviations

ALF	average liquid fraction
CSP	concentrating solar power
HTF	heat transfer fluid
LF	liquid fraction
LHS	latent heat storage
PCM	phase change material
SHS	sensible heat storage
TES	thermal energy storage

achieve the same effects. The continuous variation of a PCM melting temperature and latent heat along the bed is neither a practical nor an economical approach. Instead, the storage system is made of number of stages. Each stage is packed with capsules containing a PCM of different melting temperature. Doing so, one establishes more uniform temperature difference between the HTF and the PCMs. Yang et al. [5] numerically investigated a heat storage tank filled with the spherical capsules of three PCMs according to their melting temperatures; which comprise a packed bed and used water as the HTF. Using a finite difference method for the numerical solution, the comparison between a single and multiple PCMs was made by evaluating the results in terms of the energy and exergy performance. The conclusions indicate that there is an advantage of using multiple materials from the energy aspect, whereas exergy efficiency is lower during the melting process. This result is possibly related to the specific model used in that work and further analysis is required. Furthermore, the solar collector used for water heating showed a higher collection efficiency when multiple PCMs are used.

Most recently, Aldoss et al. [6] used spherical capsules filled with PCM of different thermo-physical properties. Spherical capsule containing paraffin 40, paraffin 50 and paraffin 60 were used in various stages along the length of bed. It was observed that an increase in the number of stages of multiple PCMs based latent heat storage system resulted into enhanced rate of charge and discharge, increased heat transfer rate and improved storage capacity. However, increasing the number of stages more than three could not enhance the system performance significantly. Gong et al. [7] presented the exergy analysis for a packed bed single-PCM TES system and compare it with the three-stage PCMs system. The overall exergy efficiency of the three-stage PCMs system was found to be 74%, higher than that of the single-PCM system. Watanabe et al. [8] developed and researched a heat storage module consisted of horizontal cylindrical capsules filled with three types of PCMs. The study proved enhanced charge and discharge rates when operated as a multi-stage PCMs compared to a latent heat storage

with only single PCM. This is due to the reason that more uniform temperature distributions exist between the heat transfer fluid and the PCM. Kousksou et al. [9] made a second law analysis of latent thermal storage for a solar system. The numerical results showed that minimum irreversibility is achieved when multi-PCMs are placed in series and linearly in the storage tank. Gracia et al. [10] reviewed and discussed different numerical methodologies available in the literature, which are used to predict the performance of latent packed bed thermal energy storage systems. Wang et al. [11] investigated the charging processes of a cylindrical heat storage capsule filled with three kinds of PCMs. Experimental results demonstrated that the charging rate is obviously enhanced. The literature review shows that the packed bed storage has been extensively studied over the years; but the temperature field inside the PCM capsules and the phase change process within the PCM capsules for single PCM and three-stage PCMs has not been deeply studied. The present study is mainly focused on this.

In this study, single-PCM of different thermo-physical properties and multi-PCM of three-stage design are investigated by using concentric-dispersion model. The concentric dispersion model is used because only this approach solves the thermal distribution inside solid particles. The phase change phenomena of PCM inside the capsules are analyzed by the apparent heat capacity method. The performance of the systems is calculated and presented in terms of storage capacity, charging and discharging temperature profile, overall thermal efficiency, exergy efficiency, utilization ratio and capacity ratio. The present work can provide insights on the optimizations of the storage system configurations and operational strategies for a better energy and exergy efficiency.

Table 1
Main characteristics and design parameters of the packed bed thermal storage system.

Parameters	Values
Height of tank (H)	7.376 m
Diameter of tank (D_{bed})	10.593 m
Porosity (ε)	0.22
Diameter of PCM capsule (D_P)	0.02653 m
Mass flow rate ($\dot{m}$)	84.5175 kg/s
Heat transfer fluid (HTF)	60% $NaNO_3$ & 40% KNO_3
Phase change material (PCM)	PCM-1, PCM-2 and PCM-3
Operating temperature (T)	288–565 °C
N_x	300
R_x	30

2. Numerical analysis

2.1. Model description

Packed bed systems provide efficient thermal storage due to their high heat transfer effectiveness. A general structure of a packed bed thermal storage system is illustrated in Fig. 1, which consists of a vertical cylindrical tank having inlet and outlet manifolds at the ends and insulating material around the vertical walls. The height of the filler region is denoted H. D_{bed} is the diameter of the cylindrical tank. The bulk of the tank is occupied by a filler material and PCM spheres, at a porosity of ε. In the present study, Table 1 summarizes the main characteristics and parameters of the packed bed thermal storage system. The properties of HTF changing with temperature can be expressed as follows [12,13].

$$\rho\ (\mathrm{kg\ m^{-3}}) = 2090 - 0.6354T\ (^{\circ}\mathrm{C}) \quad (1)$$

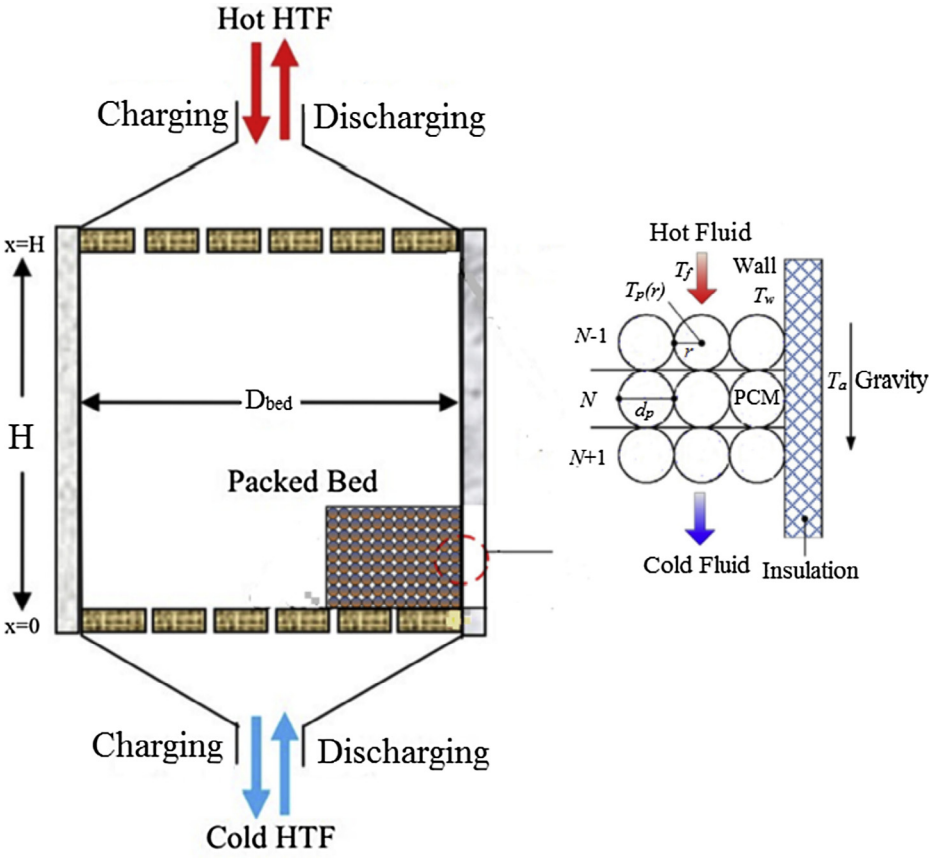

Fig. 1. Schematic diagram of packed bed thermal storage system.

$$\mu\ (\mathrm{Ns\,m^{-2}}) = [22.714 - 0.12T\ (^{\circ}\mathrm{C}) + 2.281 \times 10^{-4}T^{2}\ (^{\circ}\mathrm{C}) - 1.474 \times 10^{-7}T^{3}\ (^{\circ}\mathrm{C})] \times 10^{-3} \quad (2)$$

$$c_p\ (\mathrm{J\,kg^{-1}\,K^{-1}}) = 1443 - 0.172T\ (^{\circ}\mathrm{C}) \quad (3)$$

$$k\ (\mathrm{W\,m^{-1}\,K^{-1}}) = 0.443 + 1.9 \times 10^{-4}T\ (^{\circ}\mathrm{C}) \quad (4)$$

In the present study, the following four different PCM distribution cases are considered as shown in Fig. 2.

(1) PCM-1: Single-PCM design, where all capsules are filled with the same PCM material with a low melting temperature.
(2) PCM-2: Single-PCM design, where all capsules are filled with the same PCM material with medium melting temperature.
(3) PCM-3: Single-PCM design, where all capsules are filled with the same PCM material with high melting temperature.
(4) Three-stage PCMs: where the bed is divided equally into three axial-sections, each section is filled with different PCM material i.e. PCM-1, PCM-2, and PCM-3 in sequence and each PCM occupies 1/3 of the bed. The arrangements are considered in this case based on the PCM melting temperature, high to low (PCM-3, PCM-2, PCM-1). The PCMs for three-stage PCMs are selected based on two parametric study i.e. PCM latent heat and melting temperature; to identify the optimal values that would maximize the energy output of the storage system. Firstly for the latent heat, the magnitude of heat of fusion inside the PCM is expressed relative to the fixed sensible heat capacity as an inverse Stefan number:

$$InvSte = \frac{Lhm}{c_{p,ave}(T_{h,f} - T_{c,f})} \quad (5)$$

Secondly for the melting temperature, the cut-off criteria for the charging and discharging processes are applied. These threshold values are characterized by the normalized temperature, which is expressed as:

$$\theta = \frac{T_p - T_{c,f}}{T_{h,f} - T_{c,f}} \quad (6)$$

where $T_{h,f}$ and $T_{c,f}$ are the charging inlet temperature and discharging inlet temperature, respectively.

The criteria for the selection of three-stage PCMs are described in details as follow:

(a) The melting point of top PCM must be greater than the discharging cut-off temperature ($T_{Dch,cut\text{-}off}$ = 493 °C and $\theta_{Dch,cut\text{-}off}$ = 0.74). As the melting point decreases, the pinch point interface travels at a higher rate towards down section of the bed. Thus, the top PCM phase transition temperature is selected to be 505 °C, which lies just above the discharging cut-off value; and corresponds to a normalized melt temperature of 0.783. The PCM latent heat of 344 kJ kg^{-1} is equivalent to *InvSte* = 1.2.
(b) The melting point of middle PCM should be between the discharging cut-off temperature ($T_{Dch,cut\text{-}off}$ = 493 °C and $\theta_{Dch,cut\text{-}off}$ = 0.74) and the charging cut-off temperature ($T_{Ch,cut\text{-}off}$ = 396 °C and $\theta_{Ch,cut\text{-}off}$ = 0.39). Thus the middle PCM phase transition temperature is selected to be 439.8 °C, which lies between the discharging cut-off value and charging cut-off value; and corresponds to a normalized melt temperature of 0.548. The PCM latent heat of 214.9 kJ kg^{-1} is equivalent to *InvSte* = 0.75.
(c) The melting point of bottom PCM should be less than the charging cut-off temperature ($T_{Ch,cut\text{-}off}$ = 396 °C,$\theta_{Ch,cut\text{-}off}$ = 0.39). Thus the bottom PCM phase transition temperature is selected as 382.1 °C, which lies just below the charging cut-off value and corresponds to a normalized melt temperature of 0.34. The PCM latent heat of 197.6 kJ kg^{-1} is equivalent to *InvSte* = 0.7.

A molten-salt HTF fills the pore volume as well as the unfilled portions at the top and bottom of the tank. During the charging process, the hot fluid is introduced from the top end, after depositing heat, leaves the packed bed through the bottom end with a lower temperature. Reversely, during the discharging process, the cold fluid enters the packed bed from the bottom and forcing out a flow at high temperature. Table 2 lists the thermo-physical properties of the used PCMs, as published by Liu et al. [14]. The selected PCMs have appropriate thermo-physical properties that suit a multi-PCM thermal energy storage design.

2.2. Packed bed model and governing equations

In order to calculate the transient temperature distribution of HTF and storage media within the packed bed system, the concentric dispersion model is employed. The concentric dispersion model treats the packed bed as an isotropic porous medium consisting of independent spherical particles [15]. The assumptions are as follows:

(1) The solid particles are identical and isotropic, and the bed porosity is uniform.
(2) The fluid exhibits dispersed plug flow and that intra-particle radially concentric conduction occurs in the solid phase.
(3) Each sphere is modeled as axisymmetric and discretized into equally spaced radial nodes.
(4) Heat losses from the top and bottom of the tank are neglected and it is assumed that the HTF is the only medium that exchanges energy with the environment through the tank wall.
(5) The properties of molten salt are constant and calculated at an average temperature, $T_{ave} = (T_{in} + T_{out})/2$ [16].
(6) Radiant heat transfer is negligible and there is no internal heat

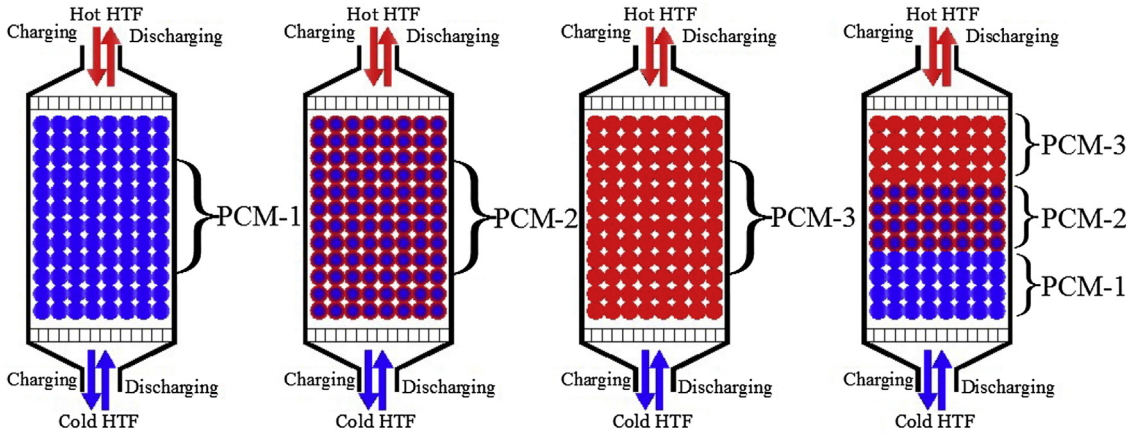

Fig. 2. Different PCMs distribution cases.

Table 2
PCMs properties.

Arrangement	PCM-1	PCM-2	PCM-3
PCM Material	PCM[a]	PCM[b]	PCM[c]
Melting temperature (°C)	382.1	439.8	505
Solidification temperature (°C)	390.9	429.8	450.1
Latent heat of fusion (kJ kg^{-1})	197.6	214.9	344
Latent heat of solidification (kJ kg^{-1})	183.7	162.9	344
Solid density (kg m^{-3})	2118	2109	2266
Liquid density (kg m^{-3})	1607	1604	2160
Solid thermal conductivity (W m^{-1} K^{-1})	1.0	1.0	2
Liquid thermal conductivity (W m^{-1} K^{-1})	1.0	1.0	1.885
Solid specific heat capacity (J kg^{-1} K^{-1})	928	1005	1338.88
Liquid specific heat capacity (J kg^{-1} K^{-1})	1035	1096	1757.28

where
[a] : 59.98 wt% $MgCl_2$ – 20.42% KCl – 19.6% NaCl.
[b] : 55 wt% $MgCl_2$ – 45% NaCl.
[c] : 35 wt% Li_2CO_3–65 wt%K_2CO_3.

generation in the bed.

In adopting the above-mentioned assumptions, the governing energy equations for the fluid and solid phases are defined respectively. Eq. (7) determines the fluid temperature in the global domain and Eq. (8) determines the solid temperature in the local domain of the sphere.

$$\frac{\partial T_f}{\partial t} = \alpha_{ax}\frac{\partial^2 T_f}{\partial x^2} - \frac{u_f}{\varepsilon}\frac{\partial T_f}{\partial x} - \frac{h_f}{c_{p,f}\rho_f \varepsilon}(T_f - T_s) - \frac{h_w D_{bed}\pi}{c_{p,f}\rho_f \varepsilon A_{bed}}(T_f - T_{\inf}) \tag{7}$$

$$\frac{\partial T_s}{\partial t} = \alpha_s\left(\frac{\partial^2 T_s}{\partial r^2} + \frac{2}{r}\frac{\partial T_s}{\partial r}\right) \tag{8}$$

where $\alpha_{ax} = (k_{eff}/\varepsilon\ \rho_f\ c_{p,f})$ and $\alpha_s = (k_s/\rho_s\ c_{p,s})$

The effective conductivity is often defined in terms of the thermal properties of the individual phases as well as the geometry of the bed. For the packed bed model, the effective thermal conductivity of the fluid phase is based on a correlation discussed in Gonzo [17] as:

$$k_{eff} = k_f\left[\frac{1 + 2\beta\varphi + (2\beta^3 - 0.1\beta)\varphi^2 + \varphi^3 0.05\exp(4.5\beta)}{1-\beta\varphi}\right] \tag{9}$$

where $\varphi = 1 - \varepsilon$ and $\beta = (k_s - 2k_f)/(k_s + 2k_f)$

The volumetric heat transfer coefficient h_f for thermal storage system can be written as [18]:

$$h_f = \frac{6(1-\varepsilon)[2 + 1.1Re_p^{0.6}Pr^{1/3}]k_f}{d_p^2} \tag{10}$$

$$Re_p = \frac{\rho_f d_p \varepsilon u_f}{\mu_f}, Pr = \frac{c_{p,f}\mu_f}{k_f} \tag{11}$$

The volumetric heat loss coefficient h_w through the wall is given by Incropera [3].

$$h_w = \frac{h'(\pi D_{bed})}{\pi D_{bed}^2/4} = \frac{4h'}{D_{bed}} \tag{12}$$

$$\frac{1}{h'} = \frac{1}{h_{in}}\frac{d_r}{D_{bed}} + \frac{D_{bed}}{2}\sum_{j=1}^{n}\frac{1}{k_f}\ln\frac{d_{j+1}}{d_j} + \frac{1}{h_{out}}\frac{d_r}{d_{n+1}} \tag{13}$$

where radiation losses from the outside wall are neglected for simplicity as their contribution to the overall heat loss is estimated to be less than 5%. For h_{out}, a correlation for natural convection on a free-standing wall given by VDI Wärmeatlas [16] is applied:

$$h_{out} = \frac{Nu_{out}k_w}{H} = \frac{\left[0.825 + 0.387[Ra.\ f(pr)]^{\frac{1}{6}}\right]^2 k_w}{H} \tag{14}$$

$$f(Pr) = \left[1 + (0.492/Pr)^{\frac{9}{16}}\right]^{\frac{16}{9}} \tag{15}$$

$$Ra = GrPr, \quad Gr = g\beta\Delta TH^3/\nu^2 \tag{16}$$

The convective heat transfer coefficient in the tank h_{in} is:

$$h_{in} = \left(\frac{k_f}{d_p}\right)(2.58Re_p^{1/3} + 0.094Re_p^{0.8}Pr^{0.4}) \tag{17}$$

The pressure drop across the thermal storage packed bed system is given by [19].

$$\Delta P = 150H\frac{(1-\varepsilon)^2}{\varepsilon^2}\frac{\mu_f u_f}{d_p^2} + 1.7H(1-\varepsilon)\frac{\rho_f u_f^2}{d_p} \tag{18}$$

2.2.1. Initial and boundary conditions

At time $t = 0$,

$$T_s = T_{ini}, \quad for \quad 0 \leqslant x \leqslant H \tag{19}$$

At time $t \geq 0$,
For the fluid phase as:

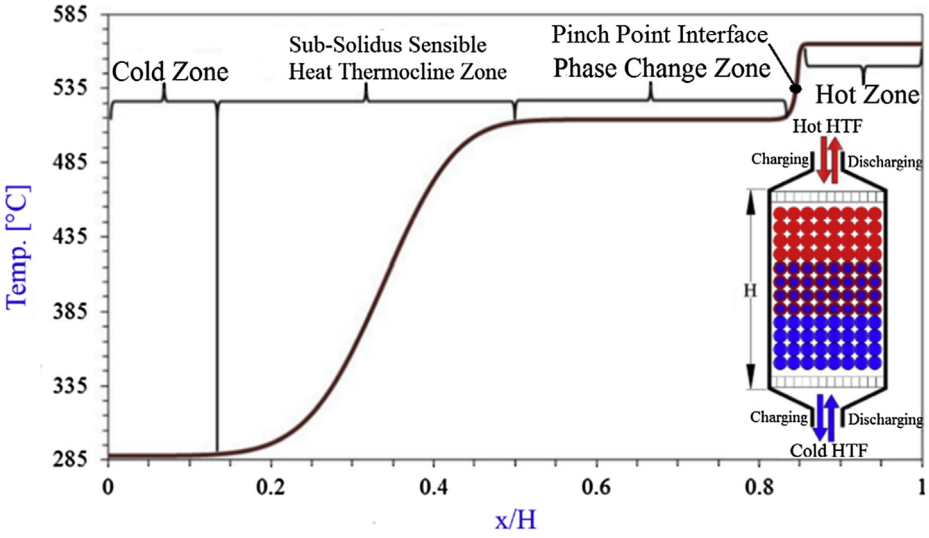

Fig. 3. Progression of the zones of a packed bed latent heat storage system during the charging process.

$$\frac{\partial T_f}{\partial x} = 0,\ at\ x = 0 \tag{20}$$

$$T_f = T_{in},\ at\ x = H \tag{21}$$

For PCM capsules at each position, the following boundary condition is used:

$$\frac{\partial T_s}{\partial r} = 0,\ at\ r = 0 \tag{22}$$

$$k_s \frac{\partial T_s}{\partial r} = h_f (T_f - T_{s,r=R_o}), at\ r = R_O \tag{23}$$

2.2.2. PCM particles as packing materials

The phase change process of PCM can be divided into three subprocesses, i.e. solid phase, phase transition and liquid phase. Latent heat is represented as a sensible heat, is spread over finite temperature difference ($T_{p2} - T_{p1}$). The thermal conductivity of the material during phase transition is assumed to be the average value of both liquid and solid phases:

(1) When PCM is in the solid phase

$$If\ T_p < T_{p1}\ c_p = c_{p,s}\ \&\ LF = 0 \quad k = k_s \tag{24}$$

(2) When PCM is in the phase transition

$$If\ T_{p1} < T_p < T_{p2}\ c_p = c_{p,app} \quad k = \frac{k_s + k_l}{2} \tag{25}$$

$$c_{p,app} = \frac{c_{p,s} + c_{p,l}}{2} + \frac{Lhm}{T_{p2} - T_{p1}} \tag{26}$$

where, Lhm is the latent heat of the PCM.

(3) When PCM is in the liquid

$$If\ T_p > T_{p2}\ c_p = c_{p,l}\ \&\ LF = 1 \quad k = k_l \tag{27}$$

2.3. Heat-exchange region

The poor utilization of latent heat at high PCM melting points is

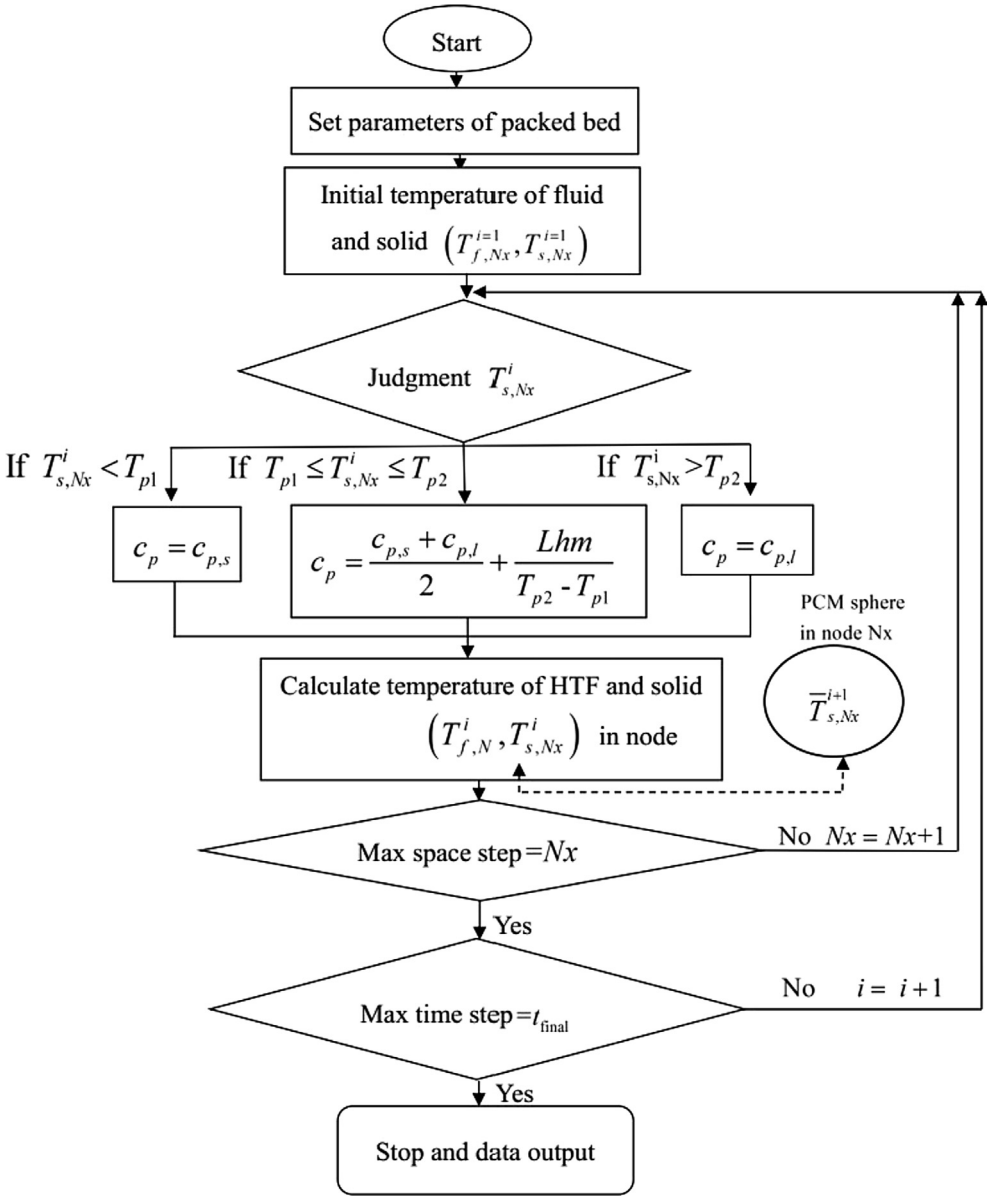

Fig. 4. Detailed numerical method procedures.

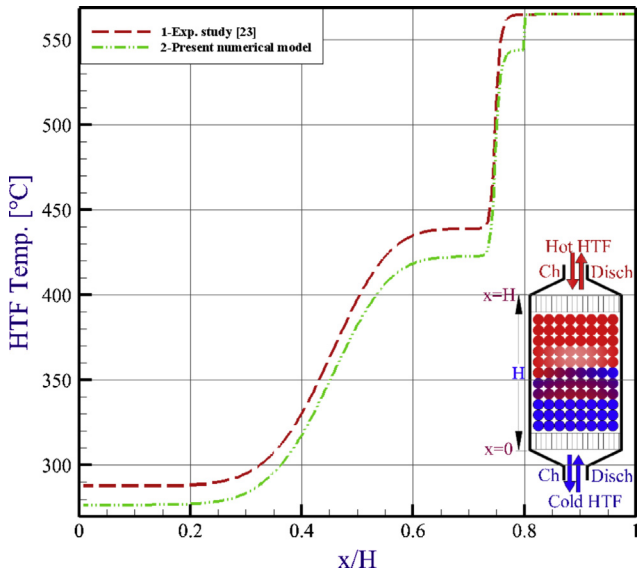

Fig. 5. Comparison between the present numerical simulation and M. Cascetta [23] experimental data of temperature profile in packed bed thermal storage system.

explained by the behavior of the heat-exchange region inside the porous bed [20]. A narrow layer of large temperature gradient develops at the interface between the hot and cold regions and is known as the thermocline or heat-exchange region; is shown in Fig. 3. The thermocline region consists of not only the sensible heat exchange zone, but is also extended to include an isothermal heat exchange zone caused by the phase change process. The relative movement of these two heat exchange segments complicates the storage and removal of thermal energy. It is heavily influenced by the thermos-physical properties of PCM, such as melting temperature and latent heat of fusion.

2.4. Numerical approach

The mathematical model developed in Section 2.2 is solved by MATLAB program using finite difference method under the fully implicit scheme. The first order upwind scheme is used to discretize the temporal and advective term in Eq. (7), while second-order central differencing is used to discretize the diffusion term. The detailed numerical method procedures are shown in Fig. 4. Let N_x nodes in the axial direction (counting in the flow direction), R_x nodes within each sphere (counting in the radial direction) and i denote the time step. The variables (T_s, T_f) are known at time step i and for all nodes N_x.

Variables at time step $i + 1$ are obtained by the following six-step procedure:

Step 1: set parameters of the packed bed and initialize the temperatures of fluid and solid.

Step 2: judge the temperature of solid PCM capsules and set the related heat capacity and thermal conductivity of PCM at different temperatures.

Step 3: finite difference method applied to the governing Eqs. (7) and (8), and can be written as:

$$\frac{T_{f,Nx}^{i+1}-T_{f,Nx}^{i}}{\Delta t}=\alpha_{ax}\frac{T_{f,Nx+1}^{i+1}-2T_{f,Nx}^{i+1}+T_{f,Nx-1}^{i+1}}{\Delta x^2}-\frac{u_f}{\varepsilon}\frac{T_{f,Nx}^{i+1}-T_{f,Nx-1}^{i+1}}{\Delta x}-\frac{h_f}{c_{p,f}\rho_f\varepsilon}(T_{s,Nx}^{i}-T_{f,Nx}^{i+1})-\frac{h_W D_{bed}\pi}{c_{p,f}\rho_f\varepsilon A_{bed}}(T_{\inf}-T_{f,Nx}^{i+1}) \quad (28)$$

The solid equation, Eq. (8), is discretized as follows:

$$\frac{T_{s,Rx}^{i+1}-T_{s,Rx}^{i}}{\Delta t}=\frac{k_s}{\rho_s c_{p,s}}\left(\frac{T_{s,Rx+1}^{i+1}-2T_{s,Rx}^{i+1}+T_{s,Rx-1}^{i+1}}{\Delta r^2}+\frac{2}{r}\frac{T_{s,Rx-1}^{i+1}-T_{s,Rx+1}^{i+1}}{2\Delta r}\right) \quad (29)$$

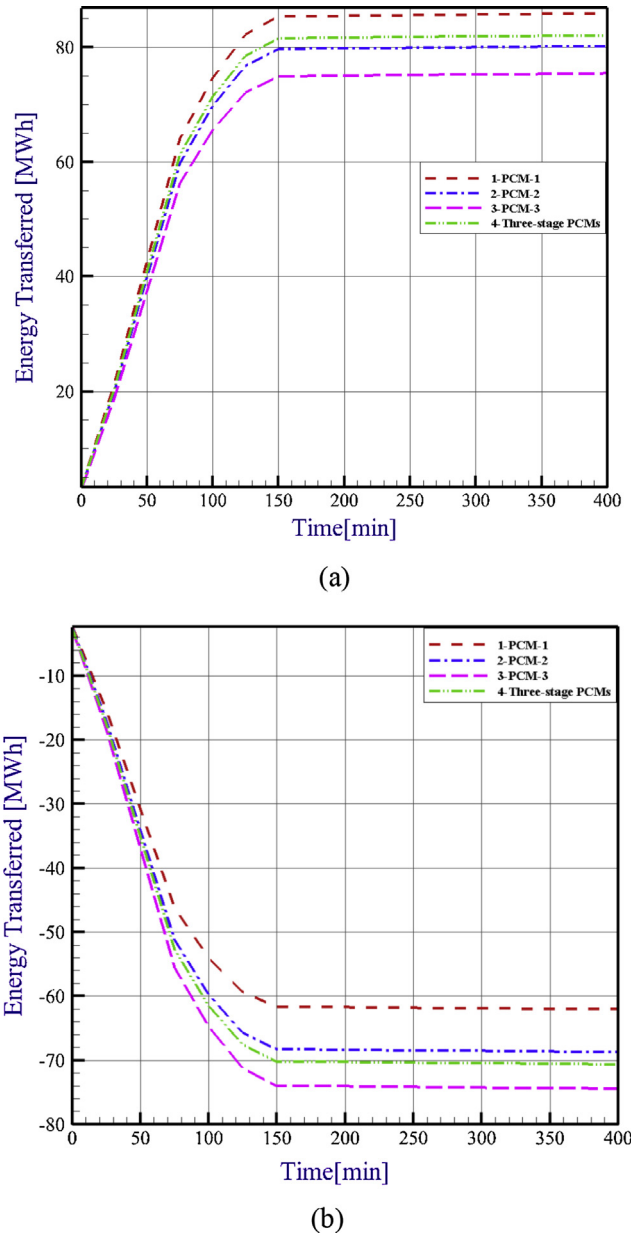

Fig. 6. Total energy transferred (a) to the bed during the charging process (b) from the bed during the discharging process.

As a result of Step1, the terms of $T_{f,Nx}^{i}$ and $T_{s,Nx}^{i}$ are known. Eqs. (28) and (29) are expressed as a tri-diagonal matrix and ($T_{f,Nx}^{i+1}$, $T_{s,Nx}^{i+1}$) can be solved by the direct finite difference approach.

Step 4: finite difference method applied to the heat transfer in PCM capsules. Eqs. (8) and, (23) are considered:

At the center node, therefore the resulting discretization is:

$$\frac{T_{s,Rx}^{i+1}-T_{s,Rx}^{i}}{\Delta t}=\frac{6k_s}{\rho_s c_{p,s}}\left(\frac{T_{s,Rx-1}^{i+1}-T_{s,Rx}^{i+1}}{\Delta r^2}\right) \quad (30)$$

The second boundary condition of the sphere is applied to the surface of the sphere:

$$k_s\frac{T_{s1}^{i+1}-T_{s2}^{i+1}}{\Delta r}=h_f(T_{f,Nx}^{i+1}-T_{s1}^{i+1}) \quad (31)$$

As $T_{s,Nx}^{i+1}$ is known from Step3, surface, and center temperature distribution of PCM $T_{s,Nx}^{i+1}$ can be calculated for this time step. Then use the volume averaged solid $\overline{T}_{s,Nx}^{i+1}$ ($\overline{T}_{s,Nx}^{i+1}=\sum_1^{Rx} T_{s,average,Rx}^{i+1}$ / Vpi) instead of the

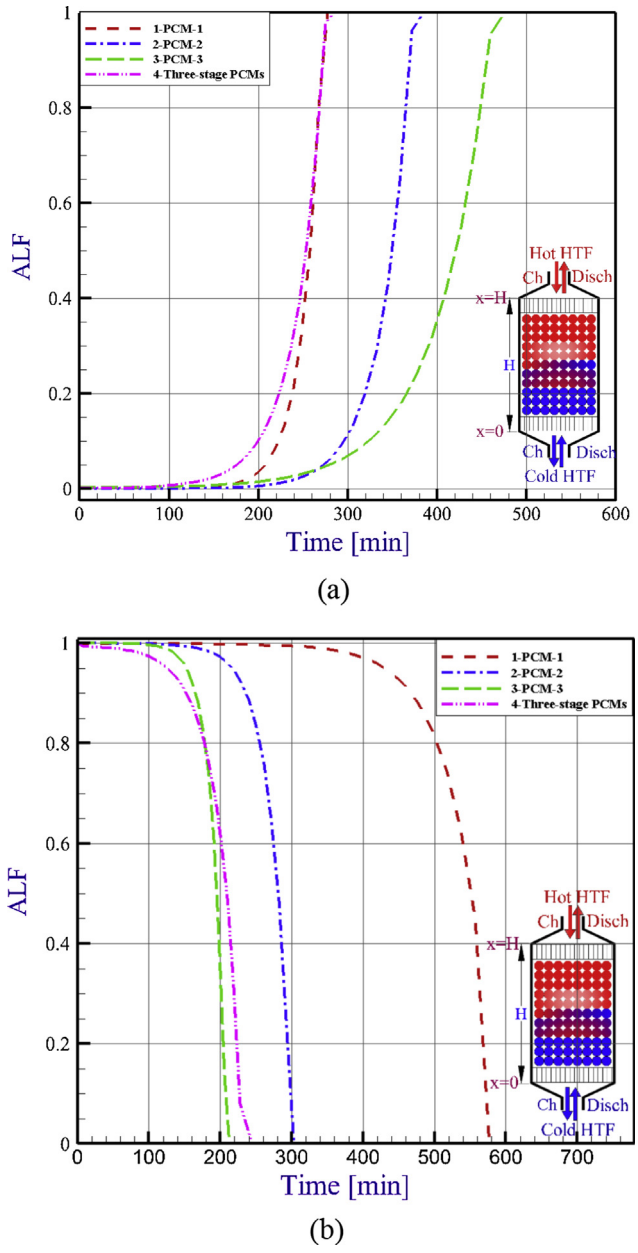

Fig. 7. The average liquid fraction for (a) charging processes (b) discharging processes.

$T_{s,Nx}^{i+1}$ temperature of PCM in the left side of Eq. (29), where V_{pi} the inner volume of the single sphere of PCM.

Step 5: repeat the Step 2–Step 4 until the number of space step reaches to N_x.

Step 6: repeat the Step 2–Step 5 until the time step reaches to t_{final}.

The simulation model is designed to calculate the axial temperature profile and quantity of energy stored within the filler material and HTF. Using this data, the net energy and exergy in and out of the system, first and second law efficiencies, capacity ratio and, utilization ratio are also determined.

3. Performance analysis

Thermal energy storage performance metrics in terms of first-law, second-law efficiencies, capacity ratio and utilization ratio provide the general measurement for TES design and analysis.

3.1. Energy and exergy efficiencies

The charging efficiency is defined as the ratio of the energy stored in the PCM at the end of the cycle to the net input and pumping energy [21]:

$$\eta_{ch} = \frac{E_{stored}}{E_{input} + E_{pump,ch}} \tag{32}$$

The discharging efficiency is defined as the fraction of the recovered energy during the discharging phase to the stored and pumping energy:

$$\eta_{disch} = \frac{E_{outflow}}{E_{stored} + E_{pump,disch}} \tag{33}$$

The overall cycle efficiency of the storage system is the ratio of the recovered energy for a single charging/discharging cycle to the input and pumping energy.

where

$$E_{pump,ch} = \sum_{i=0}^{t\ ch} (\Delta P \dot{m} \Delta t)/\rho. \tag{34}$$

$$E_{stored} = E_{stored\ after\ ch} - E_{stored\ before\ ch} \tag{35}$$

$$\eta_{overall} = \frac{E_{outflow}}{E_{input} + E_{pump,ch} + E_{pump,disch}} \tag{36}$$

The overall exergy efficiency of the storage system for a complete charging and discharging cycle is the ratio of net exergy recovered to the net exergy supplied.

$$\eta_{II} = \frac{Ex_{rec,f,net}}{Ex_{sup,f,net}} \tag{37}$$

where $Ex_{rec,f,net}$ and $Ex_{sup,f,net}$ is calculated from the following equations.

$$Ex_{rec,f,net} = \int_{t_{initial,dch}}^{t_{final,dch}} \dot{m}_f c_{p,f} \left(T_{f,out} - T_{f,inlet} - T_{inf} \ln\left(\frac{T_{f,out}}{T_{f,inlet}} \right) \right)] dt \tag{38}$$

$$Ex_{sup,f,net} = \int_{t_{initial,ch}}^{t_{final,ch}} \dot{m}_f c_{p,f} \left(T_{f,in} - T_{f,out} - T_{inf} \ln\left(\frac{T_{f,in}}{T_{f,out}} \right) \right)] dt \tag{39}$$

3.2. Capacity ratio

The capacity ratio describes the amount of energy stored compared to the theoretical maximum energy that can be stored during the charging process.

$$Capacity\ ratio = \sigma = \frac{E_{stored}}{E_{stored}^{max}} \tag{40}$$

To calculate the energy stored in each filler sphere, the model determines whether the control volume of each radial node is in the solid, liquid, or phase transition. If the PCM temperature falls within the predefined phase change temperature range, the liquid fraction is determined as.

$$Liquid\ Fraction = LF = \frac{T_p - T_{p1}}{T_{p2} - T_{p1}} \tag{41}$$

3.3. Utilization ratio

The utilization ratio characterizes the amount of energy that is extracted versus the maximum potential stored energy that could be recovered during the discharging process if the PCM were to be cooled to the initial bed temperature [22].

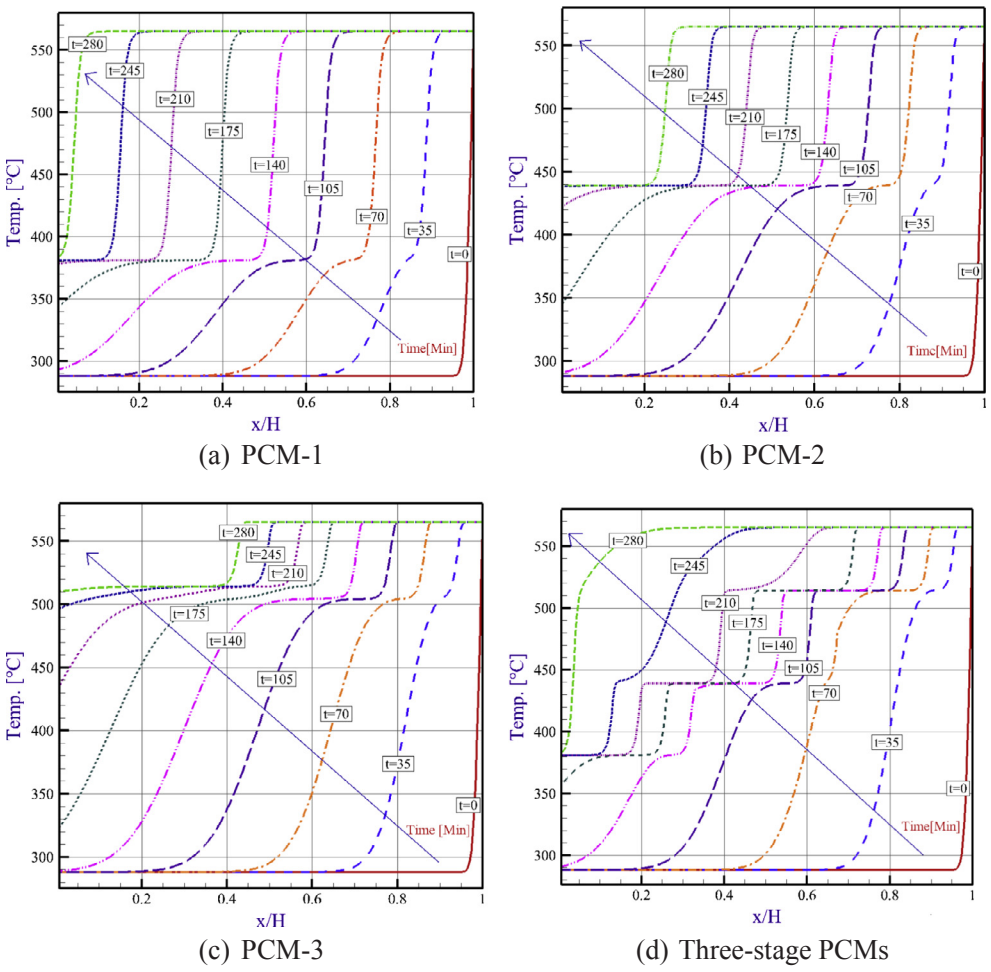

Fig. 8. Comparison of charging HTF-temperature profile of a single-PCM-1, PCM-2, PCM-3, and Three-stage PCMs.

$$Utilization\ ration = \gamma = \frac{E_{disch}}{E_{stored}^{max}} \tag{42}$$

where the discharging energy is determined by calculating the difference between the energy stored at the end of the charging cycle and the energy remaining in the filler material after the discharging cycle:

$$E_{disch} = E_{stored\ after\ ch} - E_{stored\ after\ disch} \tag{43}$$

The maximum possible storage capacity of the system is defined as:

$$E_{stored}^{max} = m_{PCM}\, c_{p,l}(T_{inlet} - T_{p2}) + m_{PCM}\,\Delta h + m_{PCM}\, c_{p,s}(T_{p1} - T_{PCM,initial}) \tag{44}$$

Eqs. (38) and (39) are calculated at the end of each minute and summed over the charging and the discharging period to calculate the total exergy supplied or recovered.

4. Results and discussion

4.1. Model validation

In order to validate the present numerical code, the differences between the numerically predicted results and the experimental results are first presented. The experimental results of Cascetta et al. [23] are used here to validate the numerical model. A packed bed thermal storage system was set up for their experiments. The storage tank was filled with alumina beads and air was used as the heat transfer fluid. The temperature profile of HTF modeled numerically at different heights during the charging process is compared with the experimental ones in Fig. 5. As shown in this figure, for the experiments, the change in HTF temperature takes place at different heights because of the temperature stratification, in accordance with the results presented by numerical simulation. The average deviations are approximately 2.32% for temperature profile around the tank height. The numerical results of the present model seem to be in good agreement with the experimental ones. That is to say, the numerical predictions of the present model are reasonable.

4.2. Storage capacity

The performances of different cases are present in terms of the total energy transferred to or from the bed as shown in Fig. 6. Fig. 6a is for the charging process, and Fig. 6b is for the discharging process. Total energy transfer measures the capacity of the storage system, and the slope of the curve represents the rate of charging or discharging process, a measure of the dynamic characteristics of the system.

Fig. 6a compares the performance of the cases during charging process in term of the total energy transferred to the bed. It indicates that the single PCM-1 attains the highest performance, the three-stage PCMs design the second and single PCM-3 the worst in the row. The three-stage PCMs case performance is the closest to the single PCM-1 performance. The single PCM-1 has the highest rate of heat transfer because of the large difference between the temperature of the HTF and the melting temperature of PCM-1. The three-stage PCMs case attains the high performance because it has the best matching melting temperature distribution with the HTF temperature profile. The other cases PCM-2 and single PCM-3, show less performance because of the low heat transfer rate between HTF and the PCM. The melting temperatures

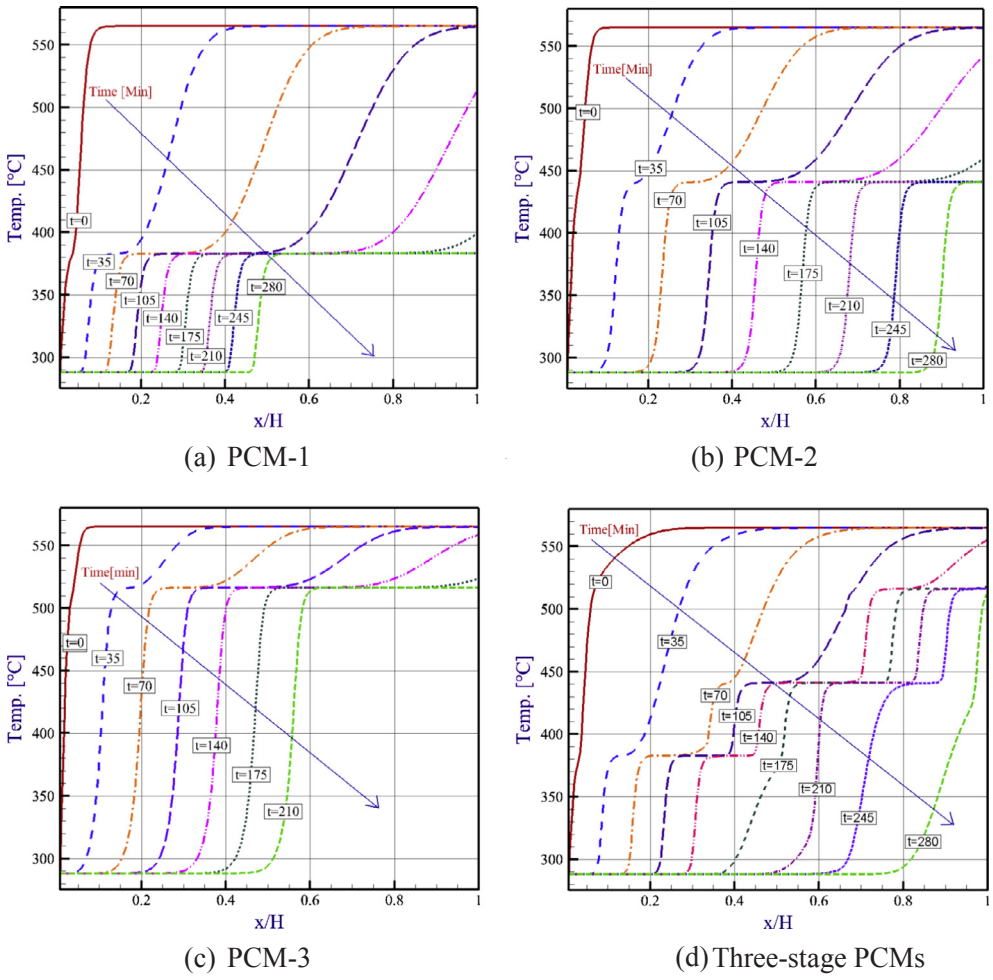

Fig. 9. Comparison of discharging HTF-temperature profile of a single-PCM-1, PCM-2, PCM-3, and Three-stage PCMs.

of the PCM in these cases are high (439.8 and 505 °C) lead to less temperature difference, thus less heat flow driving force.

Fig. 6b shows the performance of the systems during the discharging process. During discharging PCM-1 case attains the highest performance followed by the three-stage PCMs design having almost the same performance. Low performance is attained by the other two cases, single PCM-2 and single PCM-3. The reason can be attributed to the availability heat flow driving force, which is the function of the temperature difference between the HTF and the PCMs. Considering the whole operation cycle (charging and discharging) of the latent thermal energy storage system, the only design that shows high performance over the whole cycle is the three-stage PCMs design.

4.3. Average liquid fraction

Fig. 7 show the performances of the average liquid fraction for different cases. Average liquid fraction indicates the rate of melting or solidification of the PCMs in the bed. The slope of the curve represents how fast the rate of charging and discharging process is occurring. The steeper slope means the better dynamic performance of the system.

Fig. 7a for the charging process indicate that the three-stage PCMs attains the highest performance, single PCM-1 design the second and single PCM-3 the worst in the row. The three-stage PCMs case performance is the closest to the single- PCM-1 performance. The three-stage PCMs case attains the high performance because it has the best matching melting temperature distribution with the HTF temperature profile. The single PCM-1 has the highest rate of heat transfer because of the large difference between the temperature of the HTF and the melting temperature of PCM-1. The other two cases of single PCM-2 and single- PCM-3, show less performance because of the low heat transfer rate between HTF and the PCM.

Fig. 7b shows the performance of the systems during the discharging process. In this study and as expected single PCM-3 case attains the highest performance followed by the three-stage PCMs design of almost the same performance. Less performance is attained by the other two cases, single PCM-1 and single PCM-2. The reasons can be attributed to the availability of heat flow driving force, which is the function of the temperature difference between the HTF and the PCMs.

4.4. Temperature profiles in packed bed

Fig. 8 provides the temporal progression of the axial HTF temperature profiles for the PCM-1, PCM-2, PCM-3 and three-stage PCMs cases during the charging process. At 0 min of charging, all four temperature profiles are equal. When three-stage PCMs are employed, melting initiates as the sub-solidus sensible heat zone approaches a new cascade. As discussed in Section 2.3, a high rate of heat transfer occurs at the pinch point interface and the HTF leaves the interface at a temperature close to the phase transition temperature. In a three-stage PCMs system, each lower PCM can take advantage of that incoming low exergy flow stream to accelerate the phase change process, promoting greater usage of latent heat as well as sensible heat. Whereas, in the single PCM cases only one high heat transfer region exists at the interface of pinch point. After 175 min, the lengthening pinch point of the single PCM case mandates that most of the PCM is in the process of changing phase, and shortly thereafter, the charging cut-off

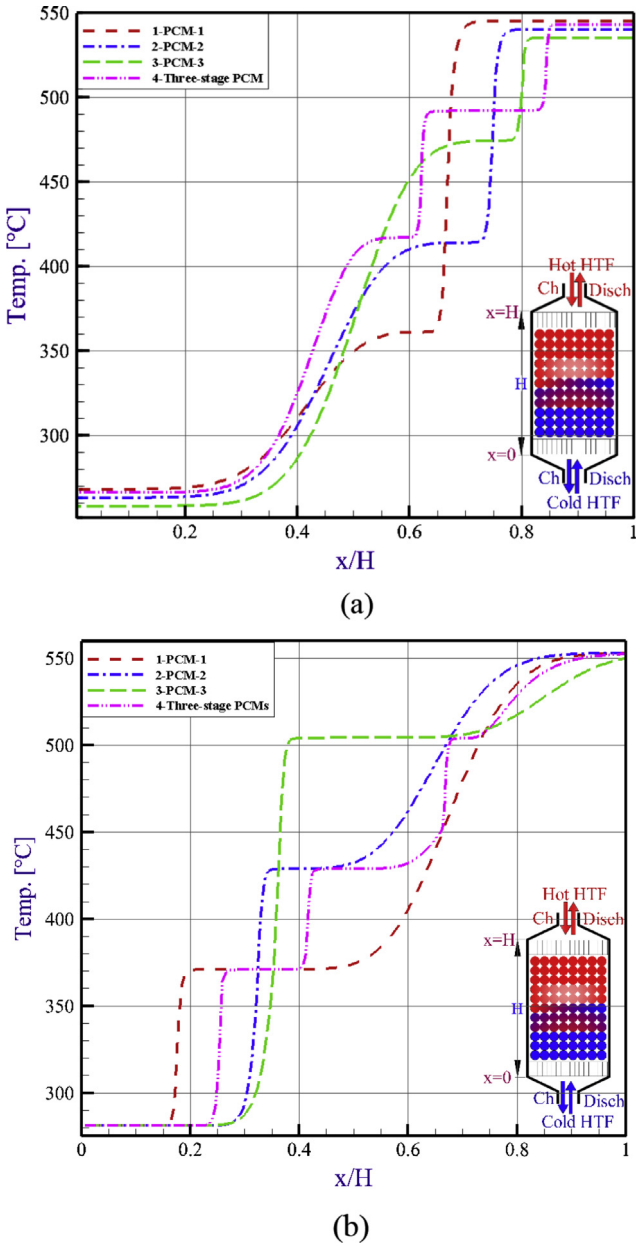

Fig. 10. The PCM temperature profile along the bed, after 100 min of (a) charging processes (b) discharging processes.

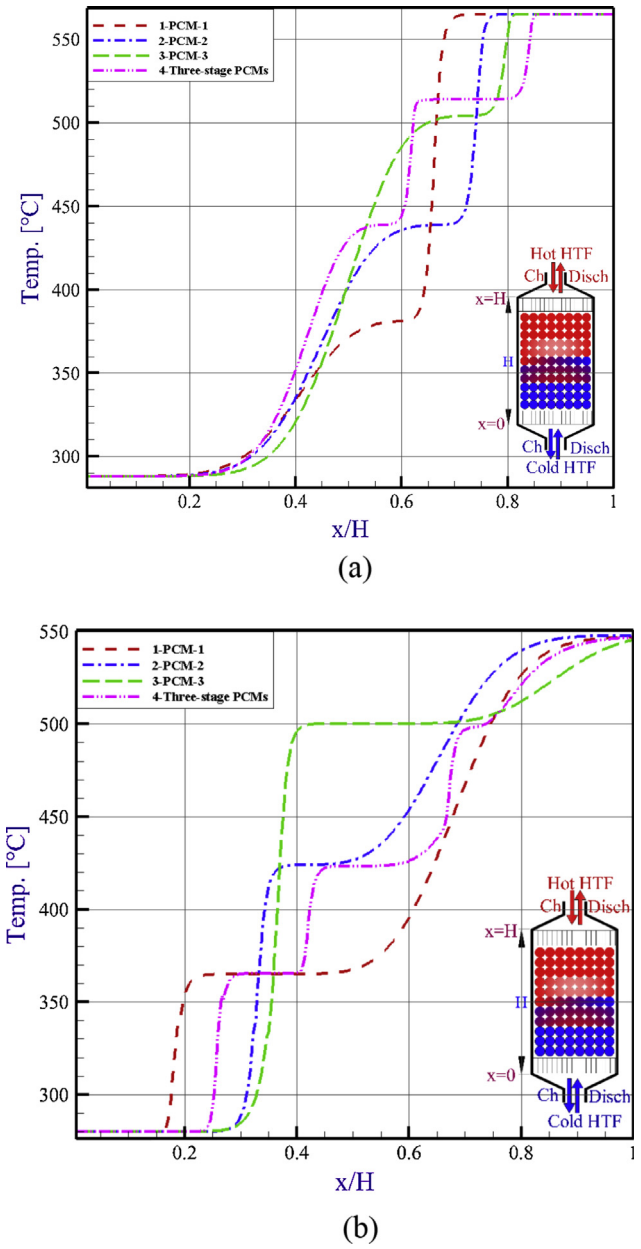

Fig. 11. The HTF temperature profile along the bed, after 100 min of (a) charging processes (b) discharging processes.

temperature is met. In the remaining two cases, the low melting PCM serves as a buffer by inhibiting the saturation condition.

At 210 min for the three-stage PCMs case, the top pinch point zone has lengthened into the bottom PCM cascade, and a fraction of the top PCM remains in the phase change process. On the other hand, simultaneously the top PCM in the three-stage PCMs system is completely melted, allowing the pinch point interface to collapse. At this moment, the hot zone is free to move at a higher velocity through the bed, as illustrated in the final charging time figures; showing that more than three-quarter of the bed in the three-stage PCMs system has reached the hot inlet temperature. When a low melting PCM is adopted, as in the single PCM-1 case, the large temperature difference between the hot inlet HTF and the phase transition temperature provides a large driving force for heat transfer, fostering rapid movement of the pinch point interface. When the melting point is high, as in the top PCM of the three-stage PCMs case, the pinch point interface travels slowly down the bed curbing the growth of hot zone. Since the three-stage PCMs has a lower fraction of the high melting PCM, it completes the melting process before the charging terminates allowing the pinch point interface to break down.

The axial HTF temperature profile for the PCM-1, PCM-2, PCM-3 and three-stage PCMs cases during discharging process is shown in Fig. 9 at different times. At 210 min for the three-stage PCMs case, the bottom pinch point zone has lengthened into the top PCM cascade, and a fraction of the top PCM remains in the phase change process. On the other hand, it is at this time that the bottom PCM in the three-stage PCMs system is completely solid, allowing the pinch point interface to collapse. At this moment, the cold zone is free to move at a higher velocity through the bed, as illustrated in the final discharging time figures, which shows that more than three-quarter of the bed in the three-stage PCMs system has reached the cold inlet temperature. When a low melting PCM is adopted, as in the single-PCM cases, the large temperature difference between the hot inlet HTF and the phase transition temperature provides a large driving force for heat transfer,

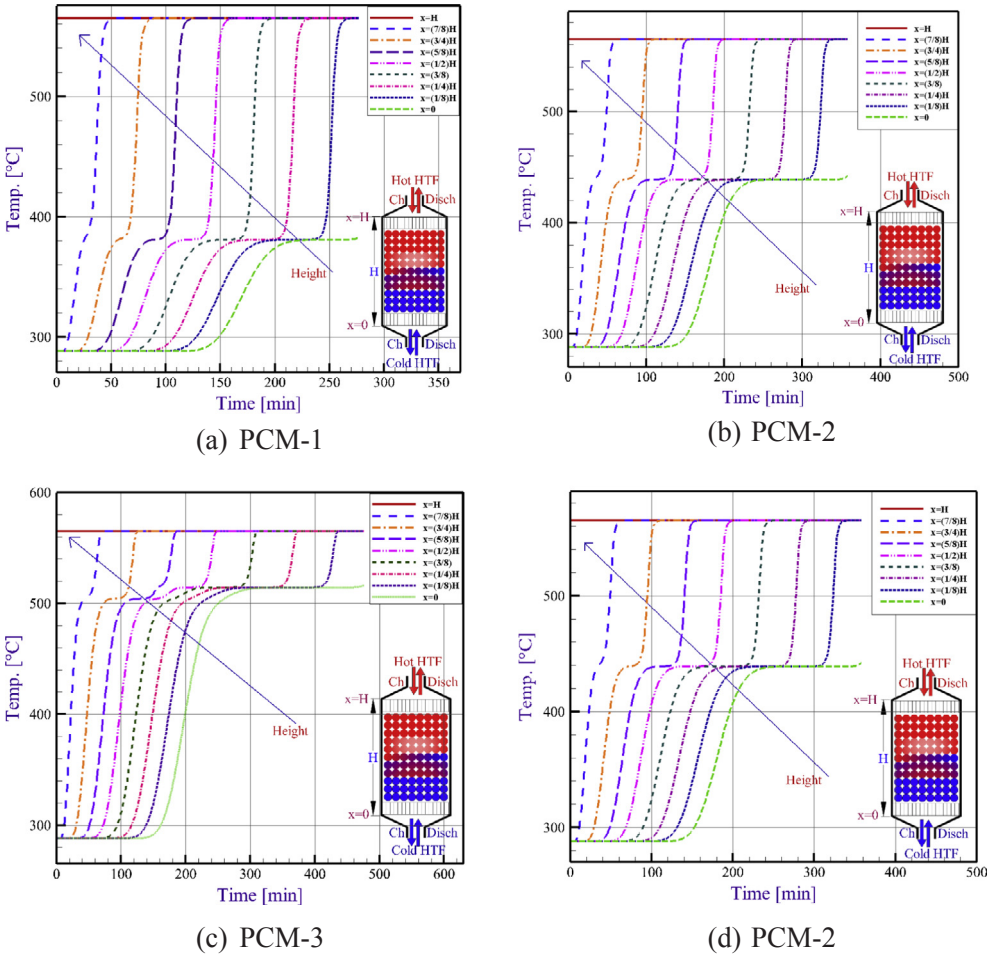

Fig. 12. Comparison of charging HTF-temperature profile vs. time of a single-PCM-1, PCM-2, PCM-3, and Three-stage PCMs.

fostering rapid movement of the pinch point interface as in the single PCM-3 case. When the solidification point is low however, as in the bottom PCM of the three-stage PCMs case, the pinch point interface travels slowly up the bed, curbing growth of the cold zone. Since the three-stage PCMs has a lower fraction of the high solidifying PCM, it completes the solidifying process before discharging terminates, allowing the pinch point interface to break down.

Fig. 10a and b show the PCM temperature profiles along the bed after 100 min of charging and discharging processes, respectively. It is clear that the behavior of the PCM in the bed is affected by its thermophysical properties. The PCM-1 (with 382.1 °C melting temperature) is the fastest to melt, followed by PCM-2 then PCM-3. The higher the temperature difference between the HTF and the PCM, the larger the heat transfer rate. The closest the melting temperature of the PCM to the HTF inlet temperature, the slower the melting process. In case of the three-stage PCMs, the melting temperature distribution matches the heat transfer temperature profile better. This improves the heat transfer process and increases the system dynamic performance.

The corresponding HTF temperature profiles along the bed are shown in Fig. 11a and b, after 100 min of charging and discharging process, respectively. During the charging process, the PCM-1 case is the fastest to charge (melt) exhibiting the highest HTF temperature, followed by PCM-2 case then the PCM-3 case. The three-stage PCMs case assumes an average behavior between the three single PCM cases and the HTF temperature shows almost constant slope along the bed. During the discharging process, the fastest to discharge (solidify) is the PCM-3 case, thus showing the lowest HTF temperature profile. The three-stage PCMs case shows the kind of constant slope HTF temperature profile, a similar behavior as during the charge process. This explains why the three-stage PCMs design maintains high performance both during charging and during discharging cycles.

Fig. 12 shows the outflow temperature during charging as a function of time for the all four cases. The slope of the HTF exit temperature curve represents the rate of the heat exchange between the HTF and the PCM. The steeper the slope, the higher the heat transfer rate, and the faster the charging. During the charging process, the single PCM-1 shows higher performance, and the single PCM-3 shows the lowest performance. During the discharging process, the single PCM-3 shows the highest performance and the single PCM-1 the lowest performance. As was discussed in the previous section, for the three-stage PCMs, the top PCM must be completely molten before the pinch point interface is collapsed and allowing the hot zone to proceed down the bed. Therefore less top PCM facilitates greater storage at the hot operating temperature. Alternatively, the bottom PCM serves as a buffer to stave off the saturation condition. This allow for the system to charge for a longer time period and recover more energy at the higher exergy state. Though three-stage PCMs produces the highest energy output, but when compared to single PCM cases, it exhibits a 44% reduction in time during which the HTF exits the system at the high exergy state.

Fig. 13 shows the outflow temperature of discharging as a function of time for all four cases. The slope of the HTF exit temperature curve represents the rate of the heat exchange between the PCM and the HTF. The steeper the slope, the higher the heat transfer rate, and the faster the discharging process. During the discharging process, the single PCM-3 shows the highest performance and the single PCM-1 the lowest performance. This analysis demonstrates that an advantage of the three-stage PCMs is to enhance energy output at the top PCM solidifying temperature. The three-stage PCMs releases HTF at the high exergy

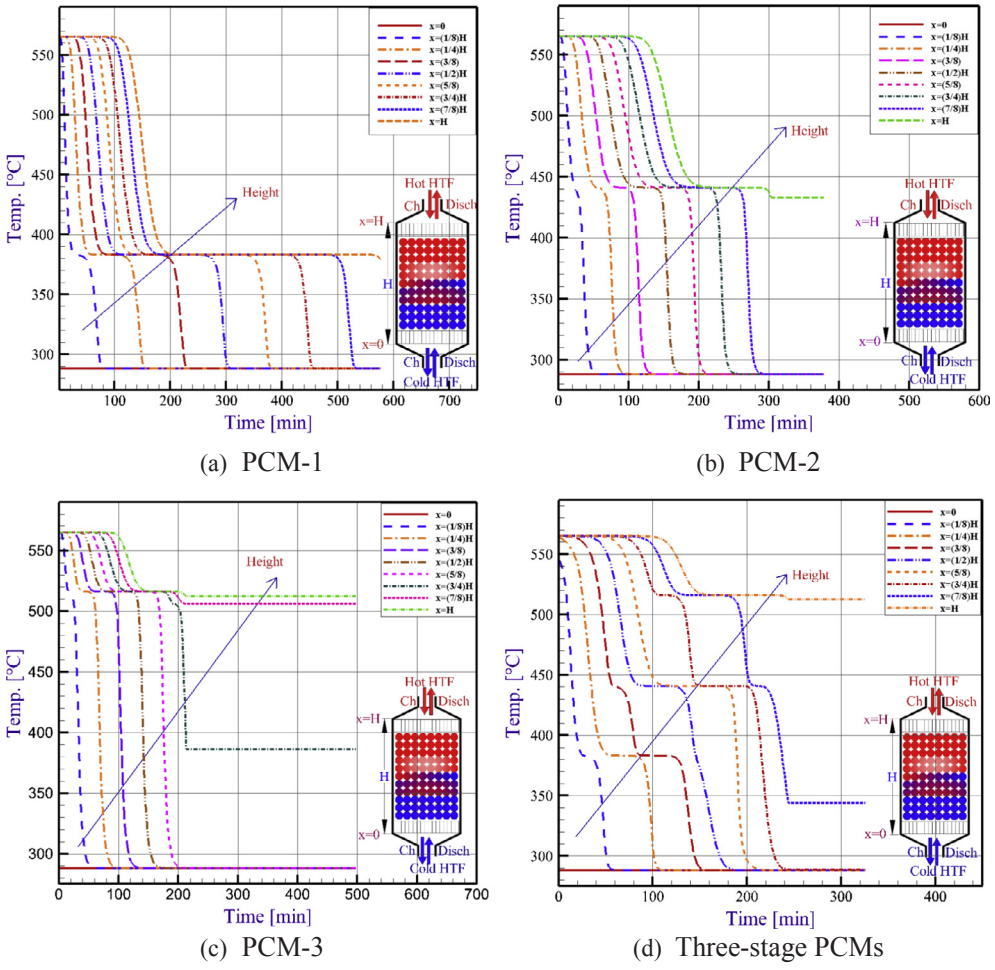

Fig. 13. Comparison of discharging HTF-temperature profile vs. time of a single-PCM-1, PCM-2, PCM-3, and Three-stage PCMs.

state in the same time frame as a single-PCM case. The three-stage PCMs benefits however, by the subsequent release of HTF at the solidifying temperature of the top PCM, which can be used to produce electricity under partial load conditions. The three-stage PCMs design shows a consistent behavior both during charging and during discharging cycles, which is in agreement with the conclusion deduced before.

4.5. Performance parameters

The performance metrics in terms of first-law, second-law efficiencies, capacity ratio and utilization ratio are used to analyze and investigate the thermal performance of cases study. Fig. 14a shows the variations in the overall energy efficiency, charging efficiency and discharging efficiency for all the considered cases. The three-stage PCMs design attains the highest performance, single PCM-1 the second and single PCM-3 the worst in the row. The single PCM-1 performance is the closest to the three-stage PCMs performance. Fig. 14b shows the variations in the utilization ratio, capacity ratio and overall exergy efficiency for all cases. The three-stage PCMs design attains the highest performance, single PCM-1 the second and single PCM-3 the worst in the row. It is found that the energy and exergy efficiencies vary between 60.6–75.76% and 41.5–75.18%, respectively. Energy efficiency is founded higher than the exergy efficiency for different cases. Energy efficiency is calculated based on the total quantity of energy transferred throughout the system. On the other hand, the exergy efficiency quantified only the useful amount of energy. To increase the exergy efficiency, it is necessary to prevent the destruction of exergy during discharging and this can be accomplished by decreasing the discharging time.

5. Conclusions

We have developed a transient Concentric-Dispersion (C-D) model to investigate the dynamic thermal performance of the single PCM and three-stage PCMs of a molten-salt packed-bed TES system containing spherical capsules filled with high-temperature PCM with different thermo-physical properties. Using the numerical model, the transient heat transfer characteristics between molten salt and PCM capsules as well as the phase change process within capsules of the three-stage PCMs unit are analyzed and compared with those of the single PCM unit with different thermo-physical properties. Then, the performance of four cases is analyzed by using the performance metrics in terms of first-law, second-law efficiencies, capacity ratio and utilization ratio. The following conclusions are drawn:

(1) The complete solidification time of PCM is too long compared to the melting time. This is due to very low heat transfer.
(2) The three-stage PCMs packed bed melts much earlier than single-type system. Because of the energy transfer from HTF to the packed bed during charging process was able to completely melt all of the PCM in the three-stage PCMs packed bed. But for single PCM packed bed, PCM at the bottom of the tank was not able to melt completely, and the highest temperature of the single PCM packed bed is much lower than that of three-stage PCMs packed bed.
(3) The three-stage PCMs unit has a considerably higher heat transfer rate than the single PCM unit during the charging-discharging

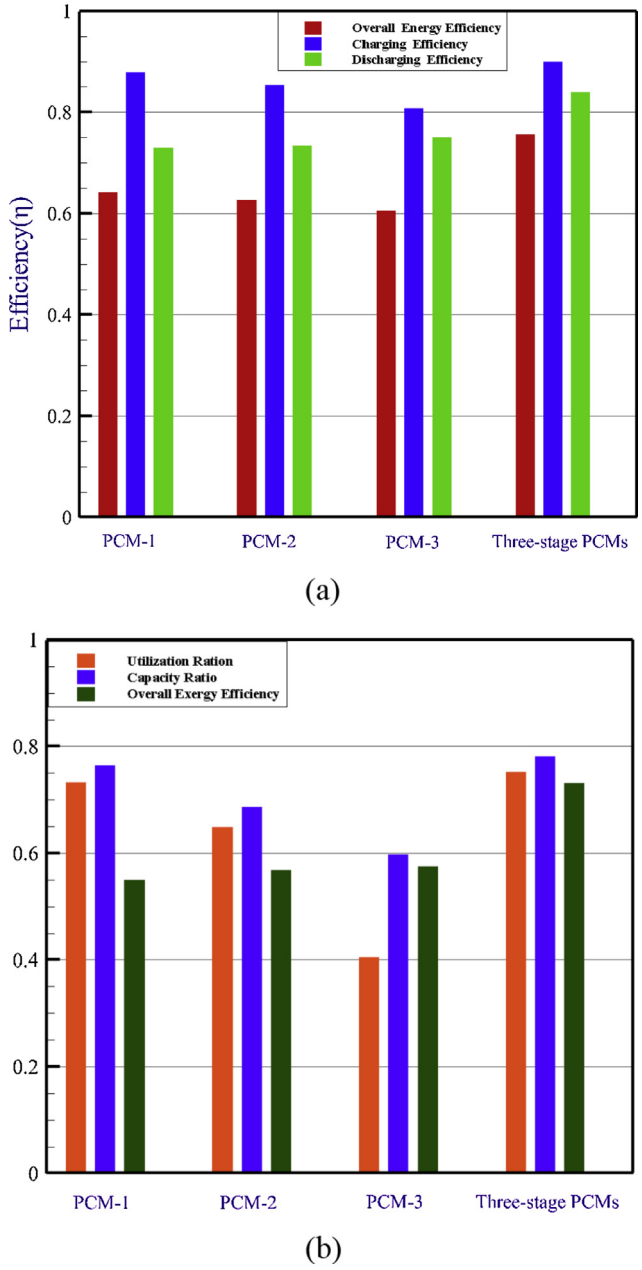

Fig. 14. Performance parameters for the four cases study of the (a) overall energy efficiency (b) utilization ratio, capacity ratio and, overall Exergy efficiency.

cycles. Because the melting temperature variation of three-stage PCMs matched the heat transfer fluid (HTF) temperature profile along the bed.

(4) The overall efficiency of the three-stage PCMs unit is higher than that of the single PCM unit during the charging-discharging cycles under the same working conditions.

Acknowledgements

This work is financially supported by the Natural Science Foundation of China (Grant No. 51536007), the Foundation for Innovative Research Groups of the National Natural Science Foundation of China (No. 51721004) and the 111 Project (B16038).

Appendix A. Supplementary material

Supplementary data associated with this article can be found, in the online version, at http://dx.doi.org/10.1016/j.applthermaleng.2018.04.122.

References

[1] S.M. Hasnain, Review on sustainable thermal energy storage technologies, part I: heat storage materials and techniques, Energy Convers. Manage. 39 (1998) 1127–1138.
[2] B. Zalba, J.M. Marin, L.F. Cabeza, H. Mehling, Review on thermal energy storage with phase change: materials, heat transfer analysis and applications, Appl. Therm. Eng. 23 (2003) 251–283.
[3] F. Opitz, P. Trefinger, Packed bed thermal energy storage model generalized approach and experimental validation, Appl. Therm. Eng. 73 (2014) 243–250.
[4] B. Xu, P.W. Li, C. Chan, Application of phase change materials for thermal energy storage in concentrated solar thermal power plants: a review to recent developments, Appl. Energy 160 (2015) 286–307.
[5] L. Yang, X. Zhang, G. Xu, Thermal performance of a solar storage packed bed using spherical capsules filled with PCM having different melting points, Energy Build 68 (2014) 639–646.
[6] T.K. Aldoss, M.M. Rahman, Comparison between the single-PCM and multi-PCM thermal energy storage design, Energy Convers. Manage. 83 (2014) 79–87.
[7] Z.X. Gong, A.S. Mujumdar, Finite element analysis of a multi-stage latent heat thermal storage system, Numer. Heat Trans. Part A 30 (1996) 669–684.
[8] T. Watanabe, H. Kikuchi, A. Kanzawa, Enhancement of charging and discharging rates in a latent heat storage system by use of PCM with different melting temperatures, Heat Recov. Syst. CHP 13 (1) (1993) 57–66.
[9] T. Kousksou, F. Strub, J. Castaing Lasvignottes, A. Jamil, J. Bedecarrats, Second law analysis of latent thermal storage for solar system, Sol. Energy Mat. Sol. Cells 91 (2007) 1275–1281.
[10] A. de Gracia, L.F. Cabeza, Numerical simulation of a PCM packed bed system: a review, Renew. Sustain. Energy Rev. 69 (2017) 1055–1063.
[11] J.F. Wang, Y.X. Ouyang, G.M. Chen, Experimental study on charging processes of a cylindrical heat storage capsule employing multi-phase-change materials, Int. J. Energy Res. 25 (5) (2001) 439–447.
[12] C. Xu, X. Li, Z. Wang, Y. He, F. Bai, Effects of solid particle properties on the thermal performance of a packed-bed molten-salt thermocline thermal storage system, Appl. Therm. Eng. 57 (2013) 69–80.
[13] X.P. Yang, X. Yang, J. Ding, Y. Shao, F.G.F. Qin, R. Jiang, Criteria for performance improvement of a molten salt thermocline storage system, Appl. Therm. Eng. 48 (2012) 24–31.
[14] M. Liu, J.C. Gomez, C.S. Turchi, N.H.S. Tay, W. Saman, F. Bruno, Determination of thermo-physical properties and stability testing of high temperature phase-change materials for CSP applications, Sol. Energy Mat. Sol. Cells 139 (2015) 81–87.
[15] N. Wakao, S. Kaguei, Heat and Mass Transfer in Packed Beds, Gordon and Breach Science Publishers, New York, 1982.
[16] VDI-Gesellschaft, VDI-Wärmeatlas, 10th ed., Springer, Berlin, 2006.
[17] E.E. Gonzo, Estimating correlations for the effective thermal conductivity of granular materials, Chem. Eng. J. 90 (2002) 299–302.
[18] N. Wakao, S. Kaguei, T. Funazkri, Effect of fluid dispersion coefficients on particle to-fluid heat transfer coefficients in packed beds: correlation of nusselt numbers, Chem. Eng. J. 34 (1979) 325–336.
[19] P. Chandra, D. Willits, Pressure-drop and heat-transfer characteristics of air rock bed thermal storage-systems, Sol. Energy 27 (1981) 547–553.
[20] S.M. Flueckiger, S.V. Garimella, Latent heat augmentation of thermocline Energy storage for concentrating solar power a system level assessment, Appl. Energy 116 (2014) 278–287.
[21] S. Jegadheeswaran, S.D. Pohekar, T. Kousksou, Exergy based performance evaluation of latent heat thermal storage system: a review, Renew. Sustain. Energy Rev. 14 (2010) 2580–2595.
[22] K. Nithyanandam, R. Pitchumani, A. Mathur, Analysis of a latent thermocline storage system with encapsulated phase change materials for concentrating solar power, Appl. Energy 113 (2014) 1446–1460.
[23] M. Cascetta, G. Cau, P. Puddu, F. Serra, A comparison between CFD simulation and experimental investigation of a packed-bed thermal energy storage system, Appl. Therm. Eng. 98 (2016) 1263–1272.